Available online at www.sciencedirect.com
ScienceDirect
Journal of Sound and Vibration 312 (2008) 195–209
JOURNAL OF SOUND AND VIBRATION
www.elsevier.com/locate/jsvi

Generation of symmetric Lamb waves by non-uniform excitations

Baruch Karp

Faculty of Aerospace Engineering, Technion—Israel Institute of Technology, Haifa 32000, Israel

Received 9 March 2007; received in revised form 8 September 2007; accepted 20 October 2007
Available online 11 December 2007

Abstract

The plane strain response of a semi-infinite, elastic strip to harmonic, symmetric, and non-uniform end excitation is investigated analytically. The solution is obtained as a series expansion of the Rayleigh–Lamb modes of the strip. The variation of the energy partition among the propagating modes with the frequency of the end excitation was found for mixed end conditions prescribed at the excited end (load and displacement types). The bi-orthogonality relation was employed in deriving the relative amplitudes of each mode to the given excitation. It was found that the far-field response of the strip is largely indifferent to whether the excitation is a displacement or stress type. The previously reported phenomenon of the existence of one dominating wave in uniform excitation is shown to extend to moderately non-uniform excitations as well. The phenomenon of complete dominance of one mode for generally non-uniform excitations was exposed.

1. Introduction

The problem of harmonic excitation of an elastic semi-infinite strip is examined in the present paper. To the best of the author's knowledge, only uniform end excitations have been addressed analytically. Torvik and McClatchey [1] investigated thoroughly the problem of a semi-infinite strip ($0 \leqslant x < \infty$) in the plane strain condition excited at its end ($x = 0$) by a harmonic, uniform, axial force with zero transverse traction (pure stress conditions) described by

$$\begin{aligned} \sigma_x^0 &= A_0 \, \mathrm{e}^{-\mathrm{i}\omega t} \\ \tau_{xy}^0 &= 0 \end{aligned} \qquad \text{at } x = 0, \tag{1}$$

where σ_x^0, τ_{xy}^0 are the axial and the shear stresses at the end, respectively, and ω the circular frequency of the excitation (the real part of the expressions is understood throughout the paper).

A similar problem of a strip excited by uniform axial displacement with zero transverse traction at the end (mixed condition)

$$\begin{aligned} u^0 &= A_0 \, \mathrm{e}^{-\mathrm{i}\omega t} \\ \tau_{xy}^0 &= 0 \end{aligned} \qquad \text{at } x = 0 \tag{2}$$

E-mail address: baruch@tx.technion.ac.il

0022-460X/$ - see front matter © 2007 Elsevier Ltd. All rights reserved.
doi:10.1016/j.jsv.2007.10.041

was solved by Gregory and Gladwell [2]. Here, u^0 is the axial displacement at the end. The energy partition among the available propagating modes was calculated as a function of the frequency of the excitation. In both Refs. [1,2], it was noticed that most of the energy propagating down the strip axis (approximately 90% of the total energy absorbed by the strip) is carried by a single mode having non-dimensional wavenumber k, which is the closest in its value to the non-dimensional excitation frequency, Ω.

In the present paper, we consider the generation of waves by *non-uniform*, harmonic, and symmetric excitations of two types of mixed end data: axial displacement with zero transversal traction (*displacement excitation*) and axial load with zero transverse displacement (*stress excitation*). The generality of the previously observed phenomenon of a single dominating wave mode carrying energy into the strip is questioned for different cases of non-uniform excitation forms. To that end, three non-uniform excitations described by simple symmetric functions were examined, as well as three special functions, having distributions identical to three particular wave modes. The far-field steady-state response of a strip to these non-uniform excitations was found analytically with the aid of the bi-orthogonality condition, which was proved to hold for Lamb waves [3]. The analysis closely follows the one given by Gregory and Gladwell [2] (with a minor change in definition of non-dimensional displacement field to be consistent with Ref. [4]).

The dominance of one mode is found to extend, in addition to when uniform excitations are applied, to moderately non-uniform excitations (parabolic and half-cosine). Generally non-uniform excitations, on the other hand, do not appear to expose the same dominance of one wave mode having $k \approx \Omega$. Further inspection of the results suggests that the two types of mixed end conditions (displacement and stress excitations), having same form, expose similar energy partitions among the propagating modes, for any excitation form.

Complete dominance of one wave mode (conveying 100% of the total energy absorbed) is found to occur for several non-uniform excitations. This happens not only when the excitation form matches exactly one of the modes, but also when they differ.

In Section 2, the standard series method solution of a rectangular waveguide is outlined. In Section 3, we derive the expressions for the calculation of the amplitudes of each propagating mode for symmetric modes for the two mixed excitation conditions. The energy partition among the propagating wave modes for various spatial distributions of end excitation for a range of frequencies is detailed in Section 4. A discussion of the results is given in Section 5.

2. Strip under harmonic excitation

A semi-infinite strip with a thickness $2h$ consists of homogeneous, isotropic, elastic material and occupies the region $x \geqslant 0$, $|y| \leqslant h$, $|z| < \infty$ as shown in Fig. 1. The strip can be held in the plane strain condition (the z coordinate not active) while the faces $y = \pm h$, $x \geqslant 0$, $|z| < \infty$ are free of tractions. At the end $x = 0$, a harmonic and symmetric (with reference to the x–z plane) excitation is applied, with circular frequency ω.

The problem is to determine the resulting steady-state response of the strip to that excitation and, in particular, to determine the portion of the energy carried by each available propagating mode as a function of the excitation frequency for several spatial forms of the end excitation.

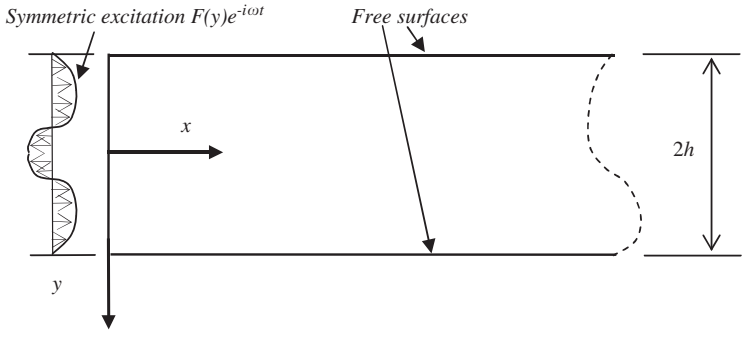

Fig. 1. Schematic view of a semi-infinite strip of thickness $2h$ on which symmetric excitation of form $\mathsf{F}(y)$ is applied at the end $x = 0$.

The equation of motion for a linearly elastic homogeneous material is

$$(\lambda+\mu)\nabla(\nabla\cdot\boldsymbol{u})+\mu\nabla^2\boldsymbol{u}=\rho\ddot{\boldsymbol{u}}, \tag{3}$$

where λ, μ are the Lame constants, ρ the material density, ∇ the gradient vector and $\boldsymbol{u}$ the displacement vector of two components

$$\boldsymbol{u}=u\mathbf{i}+v\mathbf{j}, \tag{4}$$

where both components u, v depend only on x and y coordinates and time, t. Here, $\mathbf{i}$, $\mathbf{j}$ are the unit vectors in the x, y directions, respectively. Assuming a solution of the form

$$\boldsymbol{u}(x,y,t)=A\boldsymbol{U}(y)\mathrm{e}^{\mathrm{i}(\xi x-\omega t)} \tag{5}$$

and imposing the stress free conditions on the long faces

$$\sigma_y=\tau_{xy}=0, \quad \text{at } y=\pm h \tag{6}$$

leads to the Rayleigh–Lamb frequency equation [5]

$$\frac{\tan\gamma h}{\tan\delta h}+\left(\frac{4\xi^2\delta\gamma}{(\xi^2-\gamma^2)^2}\right)^{\pm1}=0, \tag{7}$$

where γ, δ are defined in Eq. (A.4) in Appendix A. Here ξ is the *wavenumber*, $\boldsymbol{U}(y)$ is the associated cross-sectional profile for both velocity components (*wave mode*), A is a complex valued amplitude, and the $(\pm)$ sign in Eq. (7) stands for symmetric and for antisymmetric fields, respectively.

Frequency equation (7) dictates a discrete relation between the frequency ω and the wavenumber ξ. For a given frequency, Eq. (7) can be fulfilled by real, complex or imaginary wavenumbers. Real wavenumbers represent *propagating waves*. Complex and imaginary wavenumbers represent *attenuating* (or *evanescent*) *waves*. Assuming this set is a complete set of solutions (e.g. Ref. [6]), displacement field (5) will take the form

$$\boldsymbol{u}(x,y,t)=\sum_n A_n\boldsymbol{U}_n(y)\,\mathrm{e}^{\mathrm{i}(\xi_n x-\omega t)} \tag{8}$$

for any frequency ω while the summation is taken over the infinite number of all wavenumbers. The real part of Eq. (8) is understood to be the desired solution. At a given frequency, there are a finite number of real wavenumbers N and an infinite number of imaginary and complex wavenumbers. Then, solution (8) can be rewritten as

$$\boldsymbol{u}(x,y,t)=\sum_{n=1}^{N}A_n\boldsymbol{U}_n(y)\,\mathrm{e}^{\mathrm{i}(\xi_n x-\omega t)}+\sum_{n=N+1}^{\infty}A_n\boldsymbol{U}_n(y)\,\mathrm{e}^{\mathrm{i}\xi_n x}\,\mathrm{e}^{-\mathrm{i}\omega t}. \tag{9}$$

Here, the first summation represents waves propagating without attenuation (elastic material is assumed) while the second term is the sum of the attenuating waves. The response of the strip far from the loaded end (far field) therefore solely consists of the propagating waves, which are the subject of the present investigation. The non-dimensional expressions for the displacement field (8) along with the expressions for the stresses, used in the sequel, are given in Appendix A.

The actual amplitude of each mode A_n in Eq. (9) as well as its very excitation depends on the particular form of the excitation applied to the strip. We assume here two *types* of mixed conditions prescribed at the end $x=0$. Axial traction with no sliding is defined by

$$\left.\begin{aligned}&\sigma_x^0=\mu A_0\mathsf{S}(y)\,\mathrm{e}^{-\mathrm{i}\omega t}\\&v^0=0\end{aligned}\right\} \quad \text{at } x=0 \quad \text{stress excitation} \tag{10}$$

and axial displacement with no shear is given by

$$\left.\begin{aligned}&u^0=A_0\mathsf{U}(y)\,\mathrm{e}^{-\mathrm{i}\omega t}\\&\tau_{xy}^0=0\end{aligned}\right\} \quad \text{at } x=0 \quad \text{displacement excitation}, \tag{11}$$

where $\mathsf{S}(y)$ and $\mathsf{U}(y)$ are the *form* functions of the excitation and A_0 the amplitude of the excitation. These two types of excitations will be referred to as stress and displacement excitations, respectively.

It is the purpose of Section 3 to derive the expressions needed to find the amplitudes of the propagating modes A_n. These amplitudes are required for the calculation of the portion of the outgoing energy in every available propagating mode for various forms of excitation. This will further be used to unveil the dependence of this energy partition on the frequency of the excitation for various forms of the excitation, $\mathsf{S}(y)$ or $\mathsf{U}(y)$ (for sake of clarity, the argument y will be omitted in Section 3).

3. Wave amplitudes and energy partition

Let us begin with the stress excitation given by Eq. (10). Using the non-dimensional expressions (detailed in Appendix A) with stresses asociated with the nth mode defined by

$$\boldsymbol{\sigma}^n(y) = \begin{Bmatrix} \sigma_x^n(y) \\ \tau_{xy}^n(y) \end{Bmatrix} = \mu \begin{Bmatrix} S_x^n(y) \\ T_{xy}^n(y) \end{Bmatrix},$$

the axial stress and the transversal displacement at the end ($x = 0$) can be expressed in terms of series solution by

$$\begin{aligned} \sigma_x^0 &= \sum_n \sigma_x^n|_{x=0} = \mu \sum_n A_n S_x^n \, \mathrm{e}^{-\mathrm{i}\omega t}, \\ v^0 &= \sum_n v^n|_{x=0} = \sum_n A_n U_y^n \, \mathrm{e}^{-\mathrm{i}\omega t}. \end{aligned} \tag{12}$$

Completeness of the series expansion is recalled here (e.g., Ref. [7]) for justification of the general validity of Eqs. (12). Combining expansion (12) with the end condition (10) will lead to

$$\begin{aligned} \sum_n A_n S_x^n &= A_0 \, \mathsf{S}(y), \\ \sum_n A_n U_y^n &= 0. \end{aligned} \tag{13}$$

Now we multiply the first of Eq. (13) by U_x^m and the second of Eq. (13) by T_{xy}^m, where m stands for mth mode, which leads to

$$\begin{aligned} \sum_n A_n S_x^n U_x^m &= A_0 \mathsf{S} U_x^m, \\ \sum_n A_n T_{xy}^m U_y^n &= 0 \end{aligned} \tag{14}$$

and integrate Eq. (14) over the cross-section to yield

$$\begin{aligned} \int_{-h}^{h} \sum_n (A_n S_x^n U_x^m) \, \mathrm{d}y &= A_0 \int_{-h}^{h} (\mathsf{S} U_x^m) \, \mathrm{d}y, \\ \int_{-h}^{h} \sum_n (A_n T_{xy}^m U_y^n) \, \mathrm{d}y &= 0. \end{aligned} \tag{15}$$

Next, we subtract the first of Eq. (15) from the second and interchange the integral and the summation operators to obtain an equation

$$\sum_n \int_{-h}^{h} (A_n T_{xy}^m U_y^n) \, \mathrm{d}y - \sum_n \int_{-h}^{h} (A_n S_x^n U_x^m) \, \mathrm{d}y = -A_0 \int_{-h}^{h} (\mathsf{S} U_x^m) \, \mathrm{d}y. \tag{16}$$

Rearranging Eq. (16) results in

$$\sum_n A_n \int_{-h}^{h} (T_{xy}^m U_y^n - S_x^n U_x^m) \, \mathrm{d}y = -A_0 \int_{-h}^{h} (\mathsf{S} U_x^m) \, \mathrm{d}y. \tag{17}$$

The bi-orthogonality property of the wave modes [2]

$$\int_{-h}^{h}(T_{xy}^{m}U_{y}^{n}-S_{x}^{n}U_{x}^{m})\,\mathrm{d}y=0\quad\text{for } n\neq m \tag{18}$$

enable one to simplify Eq. (17) by retaining on the left-hand side only terms with $m=n$ and allowing omission of the summation over n

$$A_m\int_{-h}^{h}(T_{xy}^{m}U_{y}^{m}-S_{x}^{m}U_{x}^{m})\,\mathrm{d}y=-A_0\int_{-h}^{h}(\mathsf{S}U_{x}^{m})\,\mathrm{d}y. \tag{19}$$

From Eq. (19), the complex coefficient A_m can be deduced directly in the form

$$\frac{A_m}{A_0}=-\frac{1}{J_m}\int_{-h}^{h}(\mathsf{S}U_{x}^{m})\,\mathrm{d}y, \tag{20}$$

where

$$J_m\equiv\int_{-h}^{h}(T_{xy}^{m}U_{y}^{m}-S_{x}^{m}U_{x}^{m})\,\mathrm{d}y. \tag{21}$$

Here, J_m and $U_x{}^m$ are both properties of the mth wave mode.

An analogous derivation for the displacement excitation (11) leads to amplitude ratios

$$\frac{A_m}{A_0}=-\frac{1}{J_m}\int_{-h}^{h}(\mathsf{U}S_{x}^{m})\,\mathrm{d}y. \tag{22}$$

The mean total rate of doing work of the external excitation (per unit length in the z direction and average over strip width $2h$) is defined by [4]

$$\langle P\rangle\equiv\frac{1}{T}\frac{1}{2h}\int_{0}^{T}\int_{-h}^{h}(\sigma\cdot\dot{\boldsymbol{u}})\,\mathrm{d}y\,\mathrm{d}t \tag{23}$$

with $T=2\pi/\omega$. For harmonic waves, Eq. (23) will take the form

$$\langle P\rangle=\sum_{n}\langle P_n\rangle=-\frac{1}{4h}\omega\mu\sum_{n}|A_n|^2\,\mathrm{Im}\{J_n\}, \tag{24}$$

where the sum is taken over the n propagating modes available at the particular frequency ω. The proportion of the energy E_m communicated by the mth propagating mode is then [2]

$$E_m\equiv\frac{\langle P_m\rangle}{\langle P\rangle}=\frac{|A_m|^2\,\mathrm{Im}\{J_m\}}{\sum_{n}|A_n|^2\,\mathrm{Im}\{J_n\}}. \tag{25}$$

Calculation of energy partition according to Eq. (25) requires finding real valued wavenumbers for any frequency by the numerical solution of Rayleigh–Lamb equation (7), evaluation of integrals (21), and either Eq. (20) or (22).

4. Results

At first, four simple excitation forms, defined by the functions F,

$$\mathsf{F}(y)=A_0\quad\text{uniform}, \tag{26a}$$

$$\mathsf{F}(y)=A_0\cos\left(\frac{\pi}{2}\frac{y}{h}\right)\quad\text{half-cosine}, \tag{26b}$$

$$\mathsf{F}(y)=A_0\left(1-\left(\frac{y}{h}\right)^2\right)\quad\text{parabolic}, \tag{26c}$$

$$\mathsf{F}(y) = A_0 \cos\left(2\pi \frac{y}{h}\right) \quad \text{two-cosine} \tag{26d}$$

were examined for both stress (10) and displacement (11) excitations. Functions described by Eqs. (26b) and (26c), for reasons to be clarified later, will be termed *moderately non-uniform* excitations. Substitution of each of these functions, in turn, into relation (20) for a stress excitation, followed by integration, lead to

$$\frac{A_m}{A_0} = -\frac{1}{J_m}\frac{4}{\pi}\left[\frac{d_1^m}{\Gamma_m}\sin\left(\frac{\pi}{2}\Gamma_m\right) + \frac{d_2^m}{\Delta_m}\sin\left(\frac{\pi}{2}\Delta_m\right)\right], \tag{27a}$$

$$\frac{A_m}{A_0} = -\frac{1}{J_m}\frac{4}{\pi}\left[\frac{d_1^m}{(1-\Gamma_m^2)}\cos\left(\frac{\pi}{2}\Gamma_m\right) + \frac{d_2^m}{(1-\Delta_m^2)}\cos\left(\frac{\pi}{2}\Delta_m\right)\right], \tag{27b}$$

$$\frac{A_m}{A_0} = \frac{1}{J_m}\frac{16}{\pi^3\Gamma_m^3\Delta_m^3}\left[d_2^m\pi\Gamma_m^3\Delta_m\cos(\frac{\pi}{2}\Delta_m) + d_1^m\Delta_m^3\left(\pi\Gamma_m\cos\left(\frac{\pi}{2}\Gamma_m\right) - 2\sin\left(\frac{\pi}{2}\Gamma_m\right)\right) - 2d_2^m\Gamma_m^3\sin\left(\frac{\pi}{2}\Delta_m\right)\right], \tag{27c}$$

$$\frac{A_m}{A_0} = \frac{1}{J_m}\frac{4}{\pi}\left[\frac{d_1^m}{(16-\Gamma_m^2)}\sin\left(\frac{\pi}{2}\Gamma_m\right) + \frac{d_2^m}{(16-\Delta_m^2)}\sin\left(\frac{\pi}{2}\Delta_m\right)\right] \tag{27d}$$

for each function (26a–d), respectively. Here, Γ_m, Δ_m, d_1^m, and d_2^m are mode-dependent variables given in Eqs. (A.6) and (A.8). Evaluation of Eq. (22) reveals that relations (27) are valid also for displacement excitation (11) with the same functions (26) after replacement of d_1^m and d_2^m by d_7^m, and d_8^m, respectively.

The relative amplitudes (27), integral (21), and the energy partition (25) were calculated for the real roots (wavenumbers) of the symmetric Rayleigh–Lamb equation (7) for Poison's ratio $v = \frac{1}{4}$ and for a non-dimensional frequency range $0 < \Omega < 8$ (the non-dimensional frequency is defined in Eq. (A.5)). The resulting frequency map is recapitulated in Appendix B for reference. Owing to linearity of the problem, together with the symmetry of boundary conditions along the long faces $y = \pm h$, the field equations are decoupled to symmetric and antisymmetric equations as evident from the Rayleigh–Lamb equation (7). Mathematically, this means that antisymmetric modes cannot contribute to a symmetrical field. Physically, that implies that symmetric excitation generates only symmetric modes. Therefore, for purely symmetric excitations examined here only symmetric fields need to be considered.

Fig. 2 shows the variation of the energy partition among the propagating modes as a function of frequency for a uniform displacement excitation (26a). This plot reproduces well the previous result given by Gregory and Gladwell [2]. Since only one propagating mode is available up to frequency 1.6371 (no energy partition takes place), all forthcoming graphs begin at frequency 1.6.

Energy partition for the case of uniform stress excitation is shown in Fig. 3. This result is to be compared (after appropriate frequency scaling) with the results for uniform displacement excitation shown in Fig. 2 and with the results for a uniform pure stress excitation (1) given by Torvik and McClatchey [1]. Except for a small frequency range, $1.63 < \Omega < 1.73$, the pattern for uniform displacement closely follows the pattern found in both of the aforementioned cases of uniform excitations. The frequency range of $1.63 < \Omega < 1.73$ is the region where three modes are available while the third mode has a negative phase velocity (see Ref. [8] for details and interpretation). Owing to the scale of the plot in Ref. [1], it is impossible to make a more detailed comparison between the two excitations in that sensitive region.

Figs. 4 and 5 trace the energy partition among the available wave modes for displacement and stress excitations with the half-cosine form (26b), respectively. Up to frequency 1.63 and above 2.5, the energy partitions for stress and for displacement excitations are similar. Although the peaks in Figs. 4 and 5 are sharper than the maxima in Figs. 2 and 3, dominance of the mode with a wavenumber equal to the frequency of excitation is preserved for this type of non-uniform excitations, except for a frequency range of $1.63 < \Omega < 2.5$.

The parabolic excitation (26c) reveals that the energy partitions are almost identical, both qualitatively and quantitatively, to the half-cosine patterns in Figs. 4 and 5. This is true even within the sensitive range $1.63 < \Omega < 1.73$ and, therefore, are not shown here. This result can be attributed to the close similarity of the excitation functions (26b) and (26c).

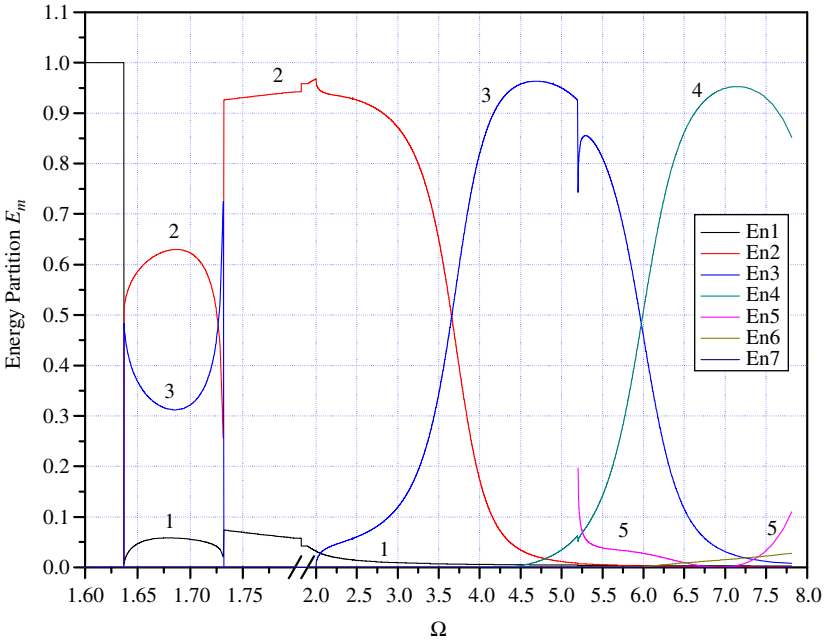

Fig. 2. Energy partition for *uniform displacement* excitation.

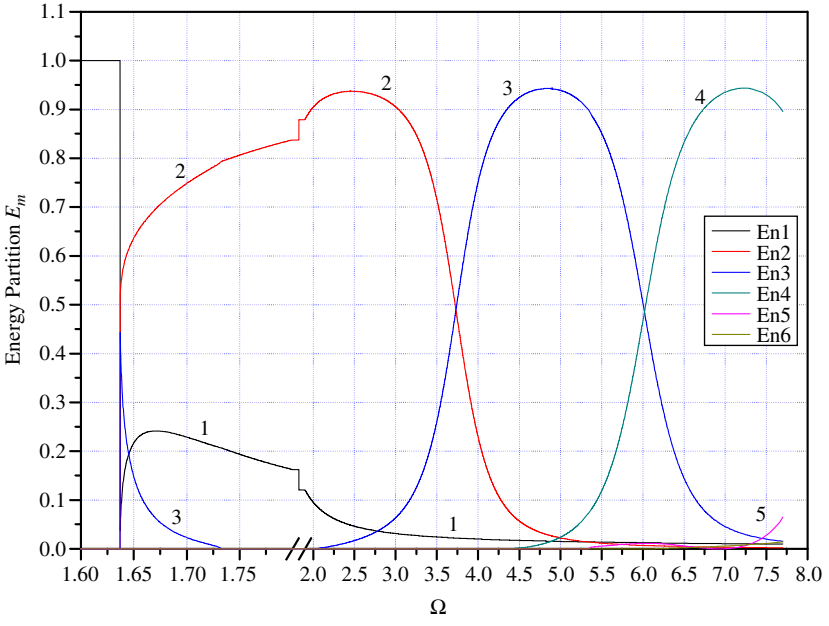

Fig. 3. Energy partition for *uniform stress* excitation.

The partition of energy for a non-uniform displacement excitation (26d) is shown in Fig. 6. Here, the pattern of energy partition markedly differs from the pattern found for uniform and moderately non-uniform excitations, with two new features. One feature is a complete dominance of one of the available modes, which conveys 100% of the absorbed energy (the third and fourth modes at frequencies 4 and 4.8, respectively). That complete dominance differs from previously observed dominances where the dominant mode delivered up to 90% of the energy. The second feature is that, at a few frequencies, dominance sets on from the very frequency

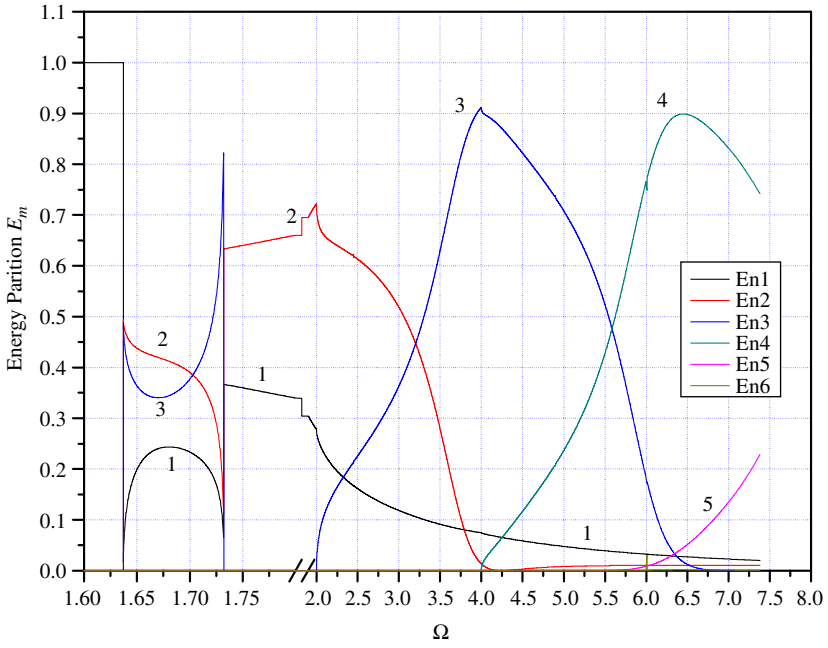

Fig. 4. Energy partition for $\cos(\pi/2\ y/h)$ *displacement* excitation.

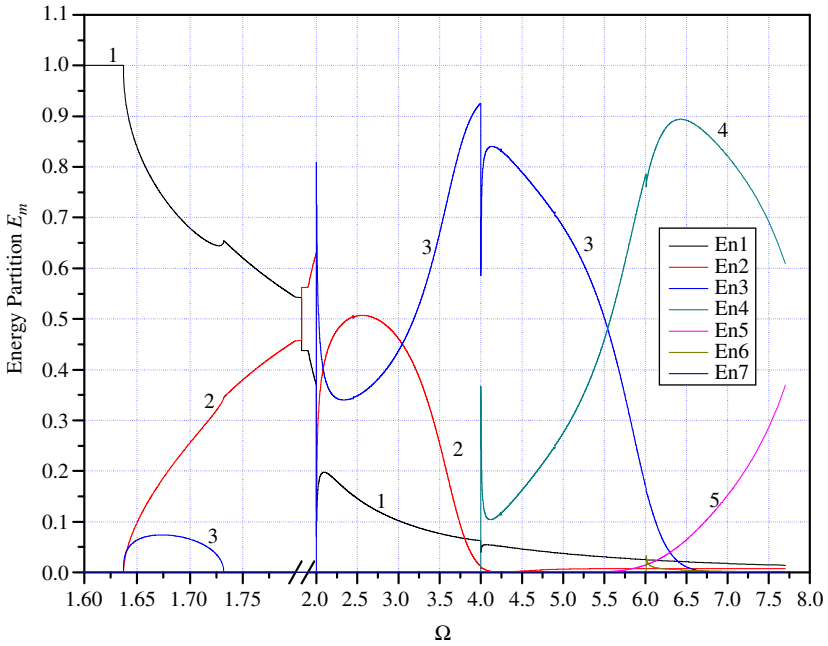

Fig. 5. Energy partition for $\cos(\pi/2\ y/h)$ *stress* excitation.

at which a new wave mode is available, and is accompanied by the complete nullification of energy delivered by all other available modes. That phenomenon occurs at frequency 4 in Fig. 6 for a displacement excitation, and for a stress excitation of the same form (26d) (not shown here).

For further examination of the phenomenon of complete dominance of a single mode, the strip response to three special excitation functions was calculated. The excitation form is taken to be identical to one of the

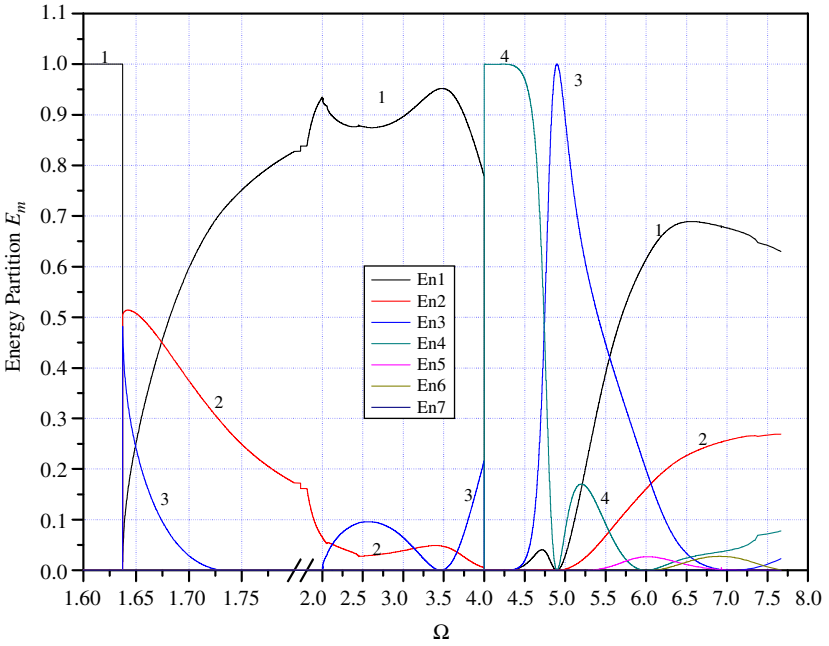

Fig. 6. Energy partition for $\cos(2\pi\ y/h)$ *displacement* excitation.

Table 1
Coefficients for stress distribution (28) for three modes available at frequency $\Omega = 1.66$

Wavenumber k_i	C_1	D_1	C_2	D_2
$k_1 = 1.44123$	14.3436	1.29384	−5.07282	1.69079i
$k_2 = 0.72436$	−1.96793	0.985774	1.34602	2.34617
$k_3 = 0.36324$	−1.18242	1.39314	0.532545	2.54433

three available modes at the frequency $\Omega = 1.66$ given by

$$\mathsf{S}(y) = C_1 \cos\left(D_1 \frac{y}{h}\right) + C_2 \cos\left(D_2 \frac{y}{h}\right), \tag{28}$$

where the coefficients C_1, C_2, D_1, and D_2, for each mode are given in Table 1. The frequency of 1.66 is chosen to lie within the range of existence of a backward wave region that appeared to be very sensitive to end data.

The energy partition for these three excitations is given in Figs. 7–9. As expected, complete dominance of one mode corresponding to its excitation form is observed at $\Omega = 1.66$. This agrees well with our experience with Fourier's theorem. Complete dominance of a single mode at higher frequencies where the form of the dominating wave mode deviates significantly from the excitation was less expected. This probably reflects the more subtle nature of bi-orthogonality relation (18) and will be further discussed in Section 5. A displacement type excitation for functions (28) reveals the same similarity between energy partition for stress and displacement type excitations. That result, along with analogous similarities for earlier evaluated functions (26), suggests that for mixed end data, both stress and displacement excitations of the same form result in a similar partition of energy.

5. Discussion

The different excitation forms examined expose rich variability in patterns of energy partition among the available wave modes. Nevertheless, some regularity can be inferred from the graphs, with additional support

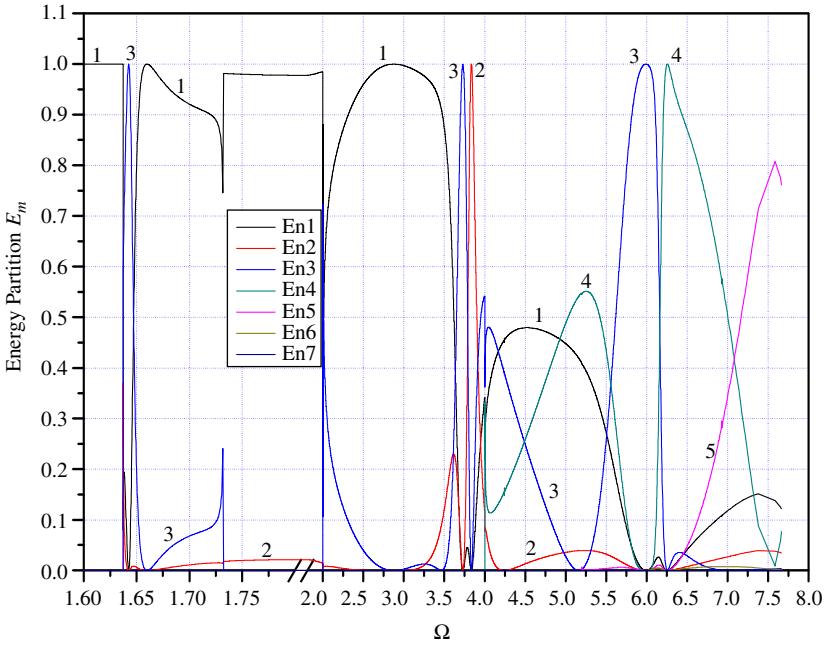

Fig. 7. Energy partition for *stress* excitation (28)—first mode.

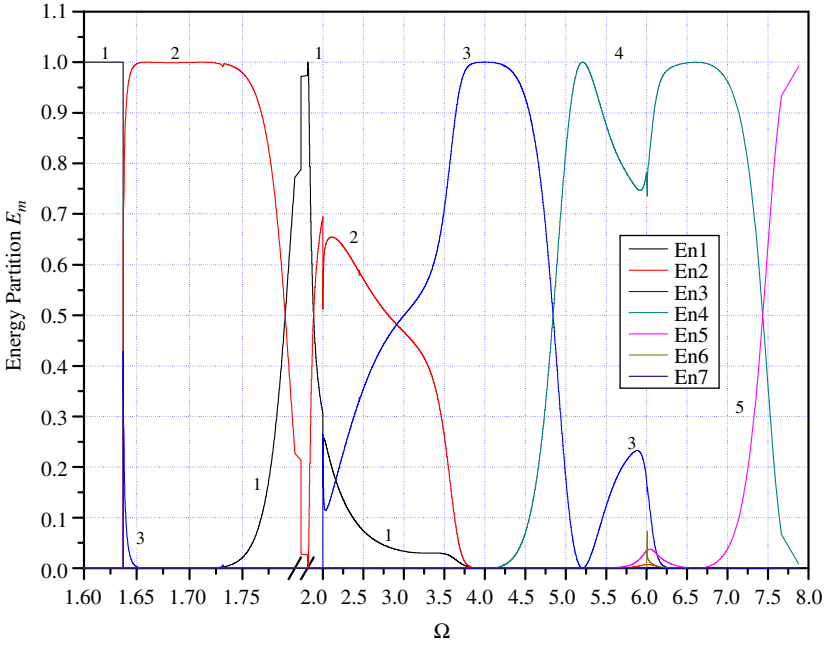

Fig. 8. Energy partition for *stress* excitation (28)—second mode.

from the following reformulation of the energy partition expression (25). Rearranging Eq. (25) will yield

$$E_m = \frac{1}{\dfrac{|A_1|^2\,\mathrm{Im}\{J_1\}}{|A_m|^2\,\mathrm{Im}\{J_m\}} + \cdots + \dfrac{|A_{m-1}|^2\,\mathrm{Im}\{J_{m-1}\}}{|A_m|^2\,\mathrm{Im}\{J_m\}} + 1 + \cdots + \dfrac{|A_n|^2\,\mathrm{Im}\{J_n\}}{|A_m|^2\,\mathrm{Im}\{J_m\}}}. \tag{29}$$

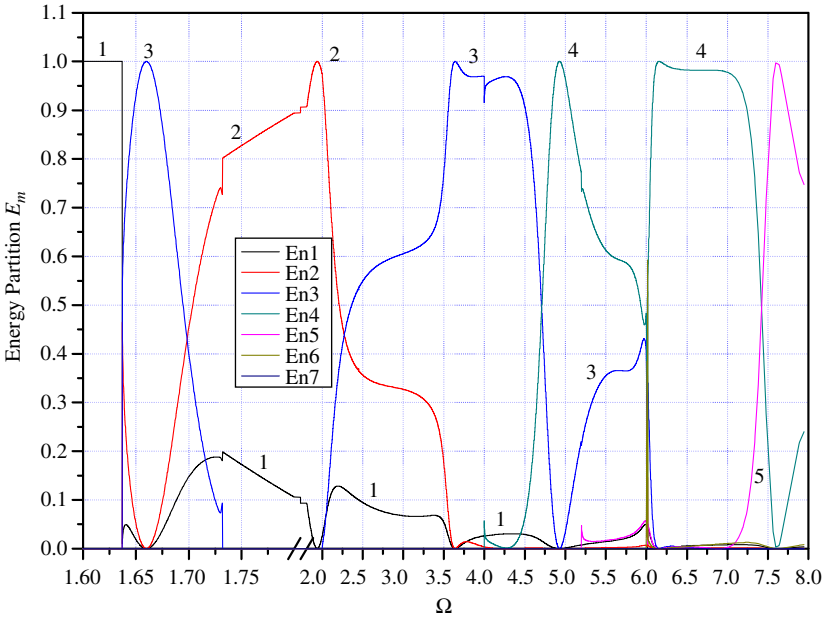

Fig. 9. Energy partition for *stress* excitation (28)—third (backward) mode.

Recalling Eq. (20), each term in the denominator of Eq. (29) can be further rewritten as

$$\frac{|A_l|^2\,\mathrm{Im}\{J_l\}}{|A_m|^2\,\mathrm{Im}\{J_m\}} = \left|\frac{J_m}{J_l}\right|^2 \frac{\mathrm{Im}\{J_l\}}{\mathrm{Im}\{J_m\}} \frac{\left|\int_{-h}^{h}(\mathsf{S}U_x^l)\,\mathrm{d}y\right|^2}{\left|\int_{-h}^{h}(\mathsf{S}U_x^m)\,\mathrm{d}y\right|^2}, \quad l = 1,2,3,\ldots,N \tag{30a}$$

for stress excitation, and as

$$\frac{|A_l|^2\,\mathrm{Im}\{J_l\}}{|A_m|^2\,\mathrm{Im}\{J_m\}} = \left|\frac{J_m}{J_l}\right|^2 \frac{\mathrm{Im}\{J_l\}}{\mathrm{Im}\{J_m\}} \frac{\left|\int_{-h}^{h}(\mathsf{U}S_x^l)\,\mathrm{d}y\right|^2}{\left|\int_{-h}^{h}(\mathsf{U}S_x^m)\,\mathrm{d}y\right|^2}, \quad l = 1,2,3,\ldots,N \tag{30b}$$

for the displacement excitation, after the use of Eq. (22). The ratios in Eqs. (30) are functions of the modal properties J_m and ${U_x}^m$ (which are frequency dependent) and of the form of the excitation, either $\mathsf{S}(y)$ or $\mathsf{U}(y)$. The reciprocal-like relations between displacement and stress excitation forms, as are evident from Eqs. (30), appear to be associated with the almost identical partition patterns for stress and displacement-type excitations of the same form.

Two deviations from perfect matching of the energy partition patterns for the two types of excitations (stress and displacement) can be noticed. One is of the kind observed at frequency 5.2 ($3\sqrt{3}$) for uniform excitations in Figs. 2 and 3 and at frequency 4 for a half-cosine excitations in Figs. 4 and 5. The differences here are limited to a very small range and can be related to the emergence of an additional propagating mode above the cut-off frequency (see frequency map in Appendix B). The second difference is in the frequency range of $1.63 < \Omega < \sqrt{3}$. This small frequency range appears to be extremely sensitive to end conditions, as is evident from all patterns shown here which exhibit a large variance in patterns within this range.

The similarity of the energy partition pattern for uniform excitations of the mixed type (stress and displacement) and the pure stress excitation (shown in Ref. [1]) are of interest. That similarity was commonly accepted as valid a few decades ago (e.g., Ref. [9, p. 19] and recently Ref. [10, p. 198]) with an illuminating work of Karal and Alterman [11]. Since there is no closed form solution for pure stress conditions (1), Torvik and McClatchey used a variational formulation to solve the problem. For the same reason, there is no

expression equivalent to Eq. (30) that could possibly illuminate that similarity. Yet, this similarity raises a question of how general that assertion can be and whether it stays valid for any excitation form.

The parabolic and the half-cosine forms show almost identical energy partitions with some deviation from the pattern found for the uniform excitations. A closer inspection reveals that the qualitative observation of a dominating mode with $k \approx \Omega$, observed first by Torvik and McClatchey for uniform excitation, is retained for these *moderately non-uniform* excitations.

The dominance-pattern characterizing the moderately non-uniform excitations is limited to up to about 90% of the total energy conveyed by one of the modes. Non-uniform excitations, on the other hand, exhibit a phenomenon of complete dominance of one of the modes conveying 100% of the energy absorbed by the strip. That phenomenon occurred both when the excitation form exactly fit one of the modes (Figs. 7–9 at frequency 1.66), as could be expected based on the experience gained through the Fourier theorem, but also for excitations with dissimilar forms (Figs. 6–9 at higher frequencies). The first case can easily be inferred from relations (29) and (30) by observing the integrals in Eqs. (30a) and (30b) to be of complete dominance for excitations which exactly fit one of the modes. Then, all other terms will have a negligible contribution to the denominator in Eq. (29). The physical reasoning behind the other instances of complete dominance observed is still to be exposed.

We conclude our discussion with a possible implication of the dominance-pattern of the mode with $k \approx \Omega$ found to characterize uniform and moderately non-uniform excitations. To that end, we consider first excitations having a frequency below $\Omega = 1.63$, where only one propagating mode is available. Now recall (e.g., Ref. [12]) that the far-field response is determined uniquely by the following quantities: frequency, material properties, and wavenumber of any available mode for a given frequency along with its amplitude (can also be inferred from Eq. (9)). For a chosen frequency (in the assumed frequency region) and symmetric excitation, a single wavenumber is obtained through the frequency equation (7). Then, the only parameter left to fix in Eq. (9) to obtain a unique result is the amplitude. The amplitude of this propagating mode can be found from Eq. (25) by

$$|A_1|^2 = \frac{\langle P \rangle}{-\frac{1}{2}\omega\mu \,\mathrm{Im}\{J_1\}}. \tag{31}$$

This leads to the conclusion that, for a given strip properties and width, given a symmetric excitation with a frequency below 1.63, the amplitude is determined by the average power of the excitation. This implies that same displacement in the far field, given by the first summation in Eq. (9), will be generated for the above set of parameters, regardless of the excitation type and its spatial distribution ($\mathsf{S}(y)$ or $\mathsf{U}(y)$).

At frequencies above 1.63, several propagating wave modes are available, making Eq. (31) invalid. Nevertheless, an equivalent result can be shown to hold for special cases. For example, at frequency $\Omega = 4$, Figs. 2–5 reveal that most of the energy for the corresponding excitation forms will be communicated by the third mode with an amplitude given by

$$|A_3|^2 = \frac{E_3\langle P \rangle}{-\frac{1}{2}\omega\mu \,\mathrm{Im}\{J_3\}}, \tag{32}$$

where E_3 is approaching 0.9. This implies that, for a given frequency, $\Omega = 4$ and, given average power of the excitation $\langle P \rangle$, the far-field response will be the same regardless of the details of the spatial distribution of the excitation, as long as the excitation form can be considered as moderately non-uniform. Based on the results obtained here, the family of "moderately non-uniform" excitations includes uniform, half-cosine, and parabolic forms of end excitations.

6. Concluding remarks

The sensitivity of the far-field response of a waveguide to non-uniform symmetric excitations has been exposed. The energy partition among the available propagating modes is given as a function of the excitation frequency. It was shown that uniform and moderately non-uniform excitations result in similar energy partition patterns, suggesting a low sensitivity of the far field to such variability in excitation. Moreover, two types of mixed end data (axial traction with transverse displacement or axial displacement with transverse

traction) induce similar responses in the far field. These findings, together with previously reported results on uniform excitation with pure end data, can be utilized to explain the available experimental data and numerical reports of a transient response of waveguides to non-uniform excitations (e.g., Refs. [13,14]).

The phenomenon of complete dominance of one mode is found to occur when various non-uniform excitations are applied to the waveguide. Only a partial explanation of that phenomenon is suggested, requiring further, more plausible, clarification.

Appendix A. Symmetric wave modes

The displacement field in a waveguide, assuming a series expansion, is written in the form

$$\boldsymbol{u}(x,y,t)=\sum_n A_n \boldsymbol{U}_n(y)\,\mathrm{e}^{\mathrm{i}(\xi_n x-\omega t)}, \tag{A.1}$$

where the summation is taken over the all admissible wavenumbers ξ_n. For a symmetric field and waveguide subjected to plain strain with lateral faces free of traction, the wave modes are given by

$$\boldsymbol{U}_n(y)=\left\{\begin{array}{c} U_x^n(y) \\ U_y^n(y) \end{array}\right\}=\left\{\begin{array}{c} \mathrm{i}\xi_n\cos(\gamma_n y)+B_n\delta_n\cos(\delta_n y) \\ -\gamma_n\sin(\gamma_n y)-\mathrm{i}B_n\xi_n\sin(\delta_n y) \end{array}\right\} \tag{A.2}$$

with

$$B_n=-2\mathrm{i}\frac{\gamma_n\xi_n}{\xi_n^2-\delta_n^2}\frac{\sin(\gamma_n h)}{\sin(\delta_n h)}=-\frac{1}{2\mathrm{i}}\frac{\xi_n^2-\delta_n^2}{\delta_n\xi_n}\frac{\cos(\gamma_n h)}{\cos(\delta_n h)} \tag{A.3}$$

and

$$\gamma_n\equiv\sqrt{\frac{\omega^2}{C_L^2}-\xi_n^2}\quad \delta_n\equiv\sqrt{\frac{\omega^2}{C_T^2}-\xi_n^2}, \tag{A.4}$$

where $2h$ is the width of the strip, and C_L and C_T are the longitudinal and transverse wave velocities in an infinite medium. It is convenient to define non-dimensional quantities as follows:

$$k_n\equiv\frac{2h}{\pi}\xi_n;\quad \Omega\equiv\frac{2h}{\pi C_T}\omega;\quad \frac{1}{\kappa^2}=\left(\frac{C_T}{C_L}\right)^2=\frac{1-2\nu}{2(1-\nu)}, \tag{A.5}$$

where ν is Poison's ratio and C_L and C_T are longitudinal and transversal velocities in infinite media, respectively. The non-dimensional parameters (A.5) for the nth mode lead to

$$\begin{aligned}\gamma_n&\equiv\frac{\pi}{2h}\Gamma_n,\quad \Gamma_n\equiv\sqrt{\frac{\Omega^2}{\kappa^2}-k_n^2},\\ \delta_n&\equiv\frac{\pi}{2h}\Delta_n,\quad \Delta_n\equiv\sqrt{\Omega^2-k_n^2}.\end{aligned} \tag{A.6}$$

Substitution of these non-dimensional quantities into relations (A.2), together with Hook's laws, will give

$$\begin{aligned}U_x^n(y)&=\frac{\pi}{2h}\left[d_1^n\cos\left(\frac{\pi}{2}\Gamma_n\frac{y}{h}\right)+d_2^n\cos\left(\frac{\pi}{2}\Delta_n\frac{y}{h}\right)\right],\\ U_y^n(y)&=\frac{\pi}{2h}\left[d_3^n\sin\left(\frac{\pi}{2}\Gamma_n\frac{y}{h}\right)+d_4^n\sin\left(\frac{\pi}{2}\Delta_n\frac{y}{h}\right)\right],\\ T_{xy}^n(y)&=\left(\frac{\pi}{2h}\right)^2\left\{d_5^n\sin\left(\frac{\pi}{2}\Gamma_n\frac{y}{h}\right)+d_6^n\sin\left(\frac{\pi}{2}\Delta_n\frac{y}{h}\right)\right\},\\ S_x^n(y)&=\left(\frac{\pi}{2h}\right)^2\left\{d_7^n\cos\left(\frac{\pi}{2}\Gamma_n\frac{y}{h}\right)+d_8^n\cos\left(\frac{\pi}{2}\Delta_n\frac{y}{h}\right)\right\}\end{aligned} \tag{A.7}$$

with

$$\begin{aligned} d_1^n &\equiv \mathrm{i}k_n & d_2^n &\equiv B_n\Delta_n, \\ d_3^n &\equiv -\Gamma_n & d_4^n &\equiv -\mathrm{i}k_nB_n, \\ d_5^n &\equiv -2\mathrm{i}k_n\Gamma_n & d_6^n &= -B_n[\Delta_n^2 - k_n^2], \\ d_7^n &\equiv -(\Omega^2 - 2\Gamma_n^2) & d_8^n &\equiv 2\mathrm{i}k_nB_n\Delta_n \end{aligned} \tag{A.8}$$

and

$$B_n = -2\mathrm{i}\frac{\Gamma_n k_n}{\Omega^2 - 2k_n^2}\frac{\sin\left((\pi/2)\Gamma_n\right)}{\sin\left((\pi/2)\Delta_n\right)} = -\frac{1}{2\mathrm{i}}\frac{\Omega^2 - 2k_n^2}{\Delta_n k_n}\frac{\cos\left((\pi/2)\Gamma_n\right)}{\cos\left((\pi/2)\Delta_n\right)}. \tag{A.9}$$

Here, the stresses are given by

$$\boldsymbol{\sigma}^n(y) = \left\{ \begin{array}{c} \sigma_x^n(y) \\ \tau_{xy}^n(y) \end{array} \right\} = \mu \left\{ \begin{array}{c} S_x^n(y) \\ T_{xy}^n(y) \end{array} \right\}. \tag{A.10}$$

Appendix B. Frequency map

Fig. B1 is the frequency map for the purely real wavenumbers k (with exchanged axes to fit the graphs in the present work) for an elastic material with Poisson's ratio of 1/4.

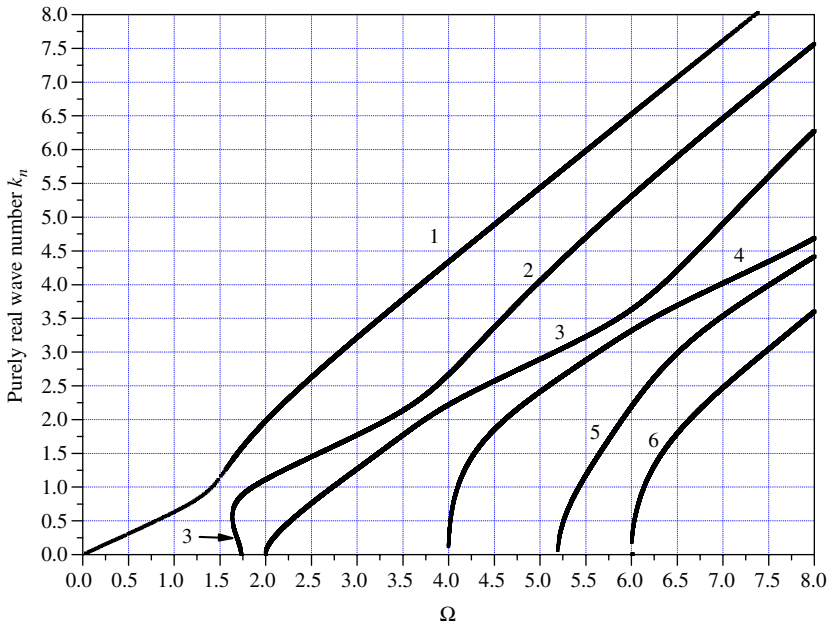

Fig. B1. Non-dimensional real wavenumbers, associated with propagating modes, with a non-dimensional frequency. This is a known Mindlin frequency map, given in the classical monographs (e.g., Refs. [4,5]) with an inverted axis. The numbers by each branch indicate the wave mode number according to Meitzler [8].

References

[1] P.J. Torvik, J.J. McClatchey, Response of an elastic plate to a cyclic longitudinal force, *Journal of the Acoustical Society of America* 44 (1968) 59–64.

[2] R.D. Gregory, I. Gladwell, The generation of waves in a semi-infinite plate by a smooth oscillating piston, *Journal of Applied Mechanics—Transactions of the ASME* 51 (1984) 787–791.

[3] W.B. Fraser, Orthogonality relation for the Rayleigh–Lamb modes of vibration of a plate, *Journal of the Acoustical Society of America* 59 (1976) 215–216.

[4] J.D. Achenbach, *Wave Propagation in Elastic Solids*, North-Holland, Amsterdam, 1973.

[5] K.F. Graff, *Wave Motion in Elastic Solids*, Clarendon Press, Oxford, 1975.

[6] J.L. Rose, *Ultrasonic Waves in Solid Media*, Cambridge University Press, Cambridge, 1999.

[7] D.E. Budreck, J.H. Rose, Elastodynamic completeness relations for scattered wavefields, *SIAM Journal on Applied Mathematics* 51 (1991) 1568–1584.

[8] A.H. Meitzler, Backward-wave transmission of stress pulses in elastic cylinders and plates, *Journal of the Acoustical Society of America* 38 (1965) 835–842.

[9] C.W. Curtis, Propagation of an elastic strain pulse in semi-infinite bar, in: N. Davids (Ed.), *International Symposium on Stress Wave Propagation in Materials*, Interscience Publishers Inc., New York, 1960, pp. 15–43.

[10] A.D. Puckett, M.L. Peterson, A semi-analytical model for predicting multiple propagating axially symmetric modes in cylindrical waveguides, *Ultrasonics* 43 (2005) 197–201.

[11] F. Karal, Z. Alterman, Far-field dependence on the end conditions in a semi-infinite elastic rod of circular cross-section, *Journal of Sound and Vibration* 17 (1971) 5–11.

[12] B. Karp, Dynamic version of Saint-Venant's principle—historical account and recent results, *Nonlinear Analysis* 65 (2005) e931–e942.

[13] O.E. Jones, F.R. Norwood, Axially symmetric cross-sectional strain and stress distributions in suddenly loaded cylindrical elastic bars, *Journal of Applied Mechanics—Transactions of the ASME* 34 (1967) 718–724.

[14] L.W. Kennedy, O.E. Jones, Longitudinal wave propagation in a circular bar loaded suddenly by a radially distributed end stress, *Journal of Applied Mechanics—Transactions of the ASME* 36 (1969) 470–478.